Available online at www.sciencedirect.com
ScienceDirect
Journal of Sound and Vibration 318 (2008) 109–130
JOURNAL OF SOUND AND VIBRATION
www.elsevier.com/locate/jsvi

Thickness optimization of a multilayered structure on the coupling surface between a structure and an acoustic cavity

T. Yamamoto[a,*], S. Maruyama[a], S. Nishiwaki[b], M. Yoshimura[b]

[a]*Nissan Motor Co. Ltd., 560-2 Okatsukoku, Atsugi-shi, Kanagawa 243-0192, Japan*
[b]*Department of Aeronautics and Astronautics, Kyoto University, Yoshida-honmachi, Sakyo-ku, Kyoto 606-8501, Japan*

Received 9 July 2007; received in revised form 31 March 2008; accepted 3 April 2008
Handling Editor: L.G. Tham
Available online 29 May 2008

Abstract

This paper describes a new design method to optimize thickness distribution of a multilayered structure which is located on the coupling surface between a structure and an acoustic cavity. The design method is based on the concept of the density approach in topology optimization incorporating a transfer matrix for a multilayered structure that includes a poroelastic media layer. The one-dimensional transfer matrix adopted here is an approximate representation addressing vibro-acoustic effects inherent in a multilayered structure, and balances calculation resources and desired accuracy. Applying the transfer matrix representation as boundary conditions on the coupling surface between a structure and an acoustic cavity, the modified equilibrium equation of the vibro-acoustic system is derived which is approximately but efficiently solved by the modal approach. In this study, the problem of minimizing the acoustic pressure within the cavity over the prescribed frequency range is formulated under the volume constraint of the poroelastic media layer. The continuous approximation of thickness distribution is assumed, and the thickness of the poroelastic media layer at each nodal point is chosen as design variables. Numerical results show that an acoustic response is significantly reduced by the optimal thickness distribution having a total weight equal to or less than that in the initial uniform thickness. These demonstrate that the proposed method is effective to design the optimal thickness distribution of a multilayered structure.

1. Introduction

This paper discusses a new design method to optimize the thickness distribution of a multilayered structure which is located on the coupling surface between a structure and an acoustic cavity to minimize sound pressure levels inside the cavity. Multilayered structures including poroelastic media for absorption and isolation are widely used in automotive industries, and these are usually applied on the coupling surface between a structure and an acoustic cavity to reduce the level of sound pressure within. To meet increasingly stringent fuel economy targets, configurations and thicknesses of multilayered structures should be designed with minimal weight, but this tends to diminish their performance in terms of decreasing sound pressure levels. Consequently, an optimization method for the design of multilayered structures is needed that can

*Corresponding author. Tel.: +81 50 2030 1008.
E-mail addresses: tks-yamamoto@mail.nissan.co.jp, ymt_takashi@ybb.ne.jp (T. Yamamoto).

0022-460X/$ - see front matter © 2008 Elsevier Ltd. All rights reserved.
doi:10.1016/j.jsv.2008.04.004

simultaneously achieve the desired requirements for weight reduction and decrease in sound pressure levels in automotive interiors.

The problem of optimizing thickness distribution of a structure has been extensively studied in the past literature in which elastic plates such as Kirchhoff plates and Mindlin–Reissner plates was mainly treated. In the beginning of 1980s, Cheng and Olhoff [1] have first demonstrated that the optimal plates may include the infinite number of the infinitely thin stiffeners and that the thickness distribution problem suffers from lack of convergence, i.e., it is ill-posed. In order to make the problem well-posed, a regularization of the problem formulation should be introduced. This regularization can be done by introducing hole-in-cell or laminated microstructure model with continuous varying volume density of the base material or stiffeners, or by introducing fictitious material model whose properties, such as elasticity or thickness, are assumed to be a continuous function of penalized material density (see, e.g., Ref. [2]). Utilizing these models in conjunction with the topology optimization method, the optimal reinforcement of a given plate was computed by Soto and Díaz [3], Díaz et al. [4], Krog and Olhoff [5], and Belblidia et al. [6], and the optimal perforated plate design was investigated by Tenek and Hagiwara [7], Lee et al. [8], and Pedersen [9].

When the regularized optimization problem is solved using the FEM, design variables are generally discretized utilizing finite element meshes prepared to solve equilibrium equations subject to optimization. If the design variables are assigned in elements, they are usually set to piecewise constant values within each element. When setting these values, sufficiently fine discretization is required in the numerical implementation, because a continuous material distribution is assumed through the regularization of the optimization problem, but applying a mesh of sufficient fineness may exceed the bounds of practical calculation resources. Furthermore, as pointed out by Sigmund and Petersson [10], numerical instabilities such as checkerboard patterns and mesh-dependencies may appear using this setting. To mitigate these numerical problems, several methods have been proposed such as filtering schemes by Sigmund [11], perimeter control by Haber [12], and local gradient constraint by Niordson [13]. To overcome the problem, Matsui and Terada [14], and Rahmatalla and Swan [15] proposed that discretized design variables be assigned to elements nodes and interpolated by a continuous function within each element. This method ensures at least C^0 continuity of design variables over the design domain, even if the adopted finite element mesh is not fine.

The problem of minimizing acoustic response has been also the subject of considerable past research. Optimal plate design is a typical approach to passively minimizing radiated sound power. Lamancusa [16] developed a general method for obtaining optimal thickness distributions of plates where radiated sound power is calculated using a discretized Rayleigh integral formulation in conjunction with a finite element solution of the structural problem with acoustic loading neglected. Wodtke and Lamancusa [17] presented a method for optimizing thickness distributions of damping layers for circular plates with respect to minimal radiated sound power in a given frequency band. More recently, Du and Olhoff [18] proposed a design method for optimal material layouts of structural panels to minimize the sound power radiated from a structural surface into ambient air, with sound pressure approximately evaluated by assuming that the surface radiates plane waves. Yoon et al. [19] presented an optimization method to minimize sound pressure levels within a prescribed acoustic cavity for a fully coupled structural–acoustic problem, by adopting a mixed displacement/pressure finite element formulation. However, optimization of multilayered structures including poroelastic media, which is usually located on boundaries between a structure and an acoustic cavity, has seldom been studied, though this material combination is widely used in industries to secure desired quietness, due to its applied simplicity. Lee et al. [20] were the first to address a design method for optimal layer sequencing of a one-dimensional multilayered structure to maximize sound transmission loss based on a topology optimization algorithm.

The dynamic responses of a multilayered structure including poroelastic media can be calculated utilizing Biot–Allard's theory proposed first by Biot [21] and developed further by Johnson et al. [22], Champoux et al. [23], and Allard [24]. This describes the coupled behavior of two phases in poroelastic media, the solid and the fluid phases. The medium in each phase is supposed to be either an elastic solid or a Newtonian fluid, and each phase can be modeled using equivalent properties which are dependent on frequency. Finite element analysis of a multilayered structure including poroelastic media by Biot–Allard's theory can predict frequency responses with an exact representation of shape and boundary conditions. Over the past several decades, there has been a great deal of effort devoted to the analysis of poroelastic media using finite element formulations.

Kang and Bolton [25] and Easwaran et al. [26] introduced a displacement-based formulation using variables for the displacements in the solid and the fluid phases. Atalla et al. [27] developed a mixed formulation using the displacements of the solid phase and the pressure of the fluid phase as variables. This mixed formulation requires only four degrees of freedom per node, while the displacement-based formulation requires six. Hence, it is advantageous from the standpoint of reduced computation time and data storage requirements. However, significant calculation time is still required to obtain frequency responses of a multilayered system when a structure and an acoustic cavity are coupled together and the degrees of freedom of the total system are huge, or when responses at numerous frequencies must be evaluated. The frequency-dependent characteristics of poroelastic media are the main cause of the onerous calculation demands.

Optimization techniques generally require many iterative calculations to obtain convergence of an objective function, which makes it all the more necessary to be able to evaluate frequency responses as quickly as possible. Frequency responses of a multilayered structure can also be obtained by the wave-based approach (see, e.g., Ref. [28]) if a structure to be solved has simple geometry or directions of the wave propagation are limited. Allard [29] and Lauriks et al. [30] have derived the transfer matrix for a poroelastic layer by applying the solutions of the Helmholtz equation for poroelastic media. The transfer matrix of a multilayered structure can be calculated analytically, which significantly reduces computation time and data storage requirements.

In this paper, we propose a new optimization method to obtain the optimal thickness distribution of a multilayered structure by applying the concept of the density approach in topology optimization and by utilizing the transfer matrix representation of a multilayered structure located on the structural–acoustic coupling surface. The rest of the paper is organized as follows: In Section 2, Biot–Allard's theory and the wave-based solution for one-dimensional problems are briefly reviewed. The transfer matrix of a multilayered structure is then implemented as boundary conditions at the coupling surface between a structure and an acoustic cavity, and the equilibrium equations of the system are derived. In Section 3, we formulate an optimization problem to obtain the optimal continuous thickness distribution for a multilayered structure. In Section 4, the computational accuracy of the frequency responses applying the transfer matrix representation of a multilayered structure is verified by comparing the results of the frequency responses obtained by the finite element formulation. Several numerical examples are finally provided to confirm the validity of the proposed optimization method.

2. Transfer matrix representation of multilayered structures

2.1. Review of Biot– Allard's theory

In this section we review the displacement-based formulation of Biot–Allard's theory for poroelastic media to highlight the validity of the descriptions used in this paper. Refer to Allard [24] for additional details. In the following, all physical quantities are expressed in the frequency domain.

As illustrated in Fig. 1, poroelastic media have two phases, one solid and the other fluid. Assuming harmonic vibration of angular frequency ω for the displacements of the solid phase u_i^s and the displacements of the fluid phase u_i^f, equilibrium equations for each phase are written as

$$\frac{\partial \sigma_{ij}^s}{\partial x_j} + \omega^2(\rho_{11}u_i^s + \rho_{12}u_i^f) = 0, \tag{1}$$

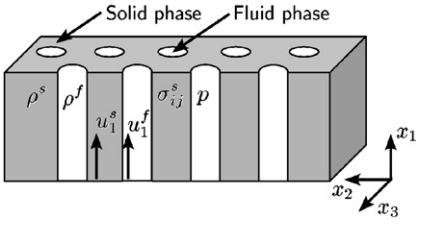

Fig. 1. A schematic view of a poroelastic medium.

$$\frac{\partial \sigma^f}{\partial x_i} + \omega^2(\rho_{12}u_i^s + \rho_{22}u_i^f) = 0, \tag{2}$$

where σ_{ij}^s and σ^f are the respective stresses in the solid and the fluid phases. Pressure in the fluid phase p^f can be written as $\sigma^f = -\phi p^f$ using the porosity ϕ. ρ_{11}, ρ_{22}, and ρ_{12} are the expressions of the complex dynamic densities considering the viscous effect induced by the relative velocities between the solid and the fluid phases:

$$\rho_{11} = (1-\phi)\rho^s + (\alpha_\infty - 1)\phi\rho^f + \frac{\sigma\phi^2}{\mathrm{j}\omega}G, \tag{3}$$

$$\rho_{22} = \phi\rho^f + (\alpha_\infty - 1)\phi\rho^f + \frac{\sigma\phi^2}{\mathrm{j}\omega}G, \tag{4}$$

$$\rho_{12} = -(\alpha_\infty - 1)\phi\rho^f - \frac{\sigma\phi^2}{\mathrm{j}\omega}G, \tag{5}$$

where j is the imaginary unit, α_∞ the tortuosity, and σ the flow resistivity, and ρ^s and ρ^f, respectively, the material densities of the solid and the fluid phases. $\sigma\phi^2 G$ is a function related to the viscous damping and G is given by

$$G = \left(1 + \frac{4\mathrm{j}\omega v}{\Lambda^2}\frac{\rho^{f2}\alpha_\infty^2}{\sigma^2\phi^2}\right)^{1/2}, \tag{6}$$

where v is the dynamic viscosity of the fluid phase, and Λ the viscous characteristic length. The constitutive laws for each phase in Biot–Allard's theory are written as

$$\sigma_{ij}^s = \{(P-2N)\varepsilon_{kk}^s + Q\varepsilon_{kk}^f\}\delta_{ij} + 2N\varepsilon_{ij}^s, \tag{7}$$

$$\sigma^f = Q\varepsilon_{kk}^s + R\varepsilon_{kk}^f, \tag{8}$$

where ε_{ij}^s and ε_{ij}^f are the respective strains of the solid and the fluid phases, δ_{ij} Kronecker's delta and N the shear modulus of the solid phase. The approximated expressions of P, Q, and R which are valid in most poroelastic media applied for absorption and insulation are derived as

$$P \simeq \frac{(1-\phi)^2}{\phi}K^f + 3\frac{1-v^s}{1+v^s}K^s, \tag{9}$$

$$Q \simeq (1-\phi)K^f, \tag{10}$$

$$R \simeq \phi K^f, \tag{11}$$

where K^s and v^s are the bulk modulus and Poisson's ratio of the solid phase, respectively. K^f is the complex dynamic bulk modulus of the fluid phase taking into account the thermal dissipation effect between the solid and the fluid phases:

$$K^f = \frac{\gamma P_0}{\gamma - (\gamma-1)(1 + (8v'/\mathrm{j}\omega\Lambda'^2)G')^{-1}}, \tag{12}$$

where γ, P_0, and v' are the specific heat ratio, the atmospheric pressure, and the thermal diffusivity, respectively. Using the thermal characteristic length Λ', G' is given by

$$G' = \left(1 + \frac{\mathrm{j}\omega\Lambda'^2}{16v'}\right)^{1/2}. \tag{13}$$

2.2. Wave-based solutions

Now we consider the one-dimensional problem in which displacements are along the x-axis. The displacement potential ψ^s and ψ^f for the solid and the fluid phases can be defined as

$$u^s = \frac{\partial \psi^s}{\partial x}, \quad u^f = \frac{\partial \psi^f}{\partial x}. \tag{14}$$

Substituting Eq. (14) into the equilibrium equations (1) and (2) and applying the constitutive laws (7) and (8), the Helmholtz equations of poroelastic media for the one-dimensional problem are derived as

$$-\omega^2(\rho_{11}\psi^s + \rho_{12}\psi^f) = P\frac{\partial^2 \psi^s}{\partial x^2} + Q\frac{\partial^2 \psi^f}{\partial x^2}, \tag{15}$$

$$-\omega^2(\rho_{12}\psi^s + \rho_{22}\psi^f) = Q\frac{\partial^2 \psi^s}{\partial x^2} + R\frac{\partial^2 \psi^f}{\partial x^2}. \tag{16}$$

Introducing $\boldsymbol{\psi} = [\psi^s \ \psi^f]^{\mathrm{T}}$, Eqs. (15) and (16) can be rewritten as

$$\frac{\partial^2 \boldsymbol{\psi}}{\partial x^2} + \mathbf{M}\boldsymbol{\psi} = 0, \tag{17}$$

where

$$\mathbf{M} = \omega^2 \begin{bmatrix} P & Q \\ Q & R \end{bmatrix}^{-1} \begin{bmatrix} \rho_{11} & \rho_{12} \\ \rho_{12} & \rho_{22} \end{bmatrix}. \tag{18}$$

Let k_i^2 $(i = 1, 2)$ be the eigenvalues for the matrix $\mathbf{M}$. The fundamental solutions for the Helmholtz equations (17) are given by $\mathrm{e}^{\pm \mathrm{j}k_i x}$. The velocities v^s and v^f, the stresses σ^s and σ^f for the solid and the fluid phases are then expressed using the unknown coefficients ξ_i and ζ_i:

$$v^s(x) = \sum_{i=1}^{2} (\xi_i \mathrm{e}^{-\mathrm{j}k_i x} - \zeta_i \mathrm{e}^{\mathrm{j}k_i x}), \tag{19}$$

$$v^f(x) = \sum_{i=1}^{2} \tau_i(\xi_i \mathrm{e}^{-\mathrm{j}k_i x} - \zeta_i \mathrm{e}^{\mathrm{j}k_i x}), \tag{20}$$

$$\sigma^s(x) = \sum_{i=1}^{2} -z_i^s(\xi_i \mathrm{e}^{-\mathrm{j}k_i x} + \zeta_i \mathrm{e}^{\mathrm{j}k_i x}), \tag{21}$$

$$\sigma^f(x) = \sum_{i=1}^{2} -\phi\tau_i z_i^f(\xi_i \mathrm{e}^{-\mathrm{j}k_i x} + \zeta_i \mathrm{e}^{\mathrm{j}k_i x}), \tag{22}$$

where

$$\tau_i = \frac{Pk_i^2 - \rho_{11}\omega^2}{\rho_{12}\omega^2 - Qk_i^2}, \tag{23}$$

$$z_i^s = (P + \tau_i Q)\frac{k_i}{\omega}, \tag{24}$$

$$z_i^f = \left(R + \frac{Q}{\tau_i}\right)\frac{k_i}{\phi\omega}. \tag{25}$$

τ_i is the ratio of the displacement of the fluid phase to the displacement of the solid phase, and z_i^s and z_i^f are, respectively, the characteristic impedance for the solid and the fluid phases.

2.3. Reduced transfer matrix of poroelastic media

As shown in Fig. 2, we consider a multilayered structure located on the coupling surface Γ^t between a structural domain Ω^e and an acoustic domain Ω^a. The multilayered structure applied here consists of a poroelastic layer and an elastic layer. If the wave normal to the coupling surface propagates dominantly in a multilayered structure, the solutions of the one-dimensional Helmholtz equations in Section 2.2 can be applied at each local point. Let x be the local coordinate normal to the coupling surface Γ^t. When $\mathbf{V}(x)$ and $\mathbf{V}_0$ are defined as

$$\mathbf{V}(x) = [v^s(x)\ v^f(x)\ \sigma^s(x)\ \sigma^f(x)]^{\mathrm{T}}, \tag{26}$$

$$\mathbf{V}_0 = [\xi_1\ \zeta_1\ \xi_2\ \zeta_2]^{\mathrm{T}}, \tag{27}$$

the solutions of the one-dimensional Helmholtz equations from Eqs. (19) to (22) are rewritten as

$$\mathbf{V}(x) = \mathbf{\Gamma}(x)\mathbf{V}_0, \tag{28}$$

where $\mathbf{\Gamma}(x)$ is a 4×4 matrix. Substituting $x = a$ and $x = b$ into Eq. (28), $\mathbf{V}(a)$ is related to $\mathbf{V}(b)$ by

$$\mathbf{V}(a) = \mathbf{\Gamma}(a)\mathbf{\Gamma}(b)^{-1}\mathbf{V}(b). \tag{29}$$

This means the transfer matrix $\mathbf{\Gamma}_{AB}$ for the poroelastic layer between a point A ($x = a$) and a point B ($x = b$) is given by

$$\mathbf{\Gamma}_{AB} = \mathbf{\Gamma}(a)\mathbf{\Gamma}(b)^{-1}. \tag{30}$$

Note that $\mathbf{\Gamma}_{AB}$ is also a 4×4 matrix and is expressed by the four components: the velocities and the stresses for each phase.

However, the transfer matrices for an elastic and an air layer are expressed by two components, the velocity and the stress. Thus, the reduced expression of a transfer matrix for a poroelastic layer that is represented by the two components, the total velocity v^p and the total stress σ^p, is convenient for multiplication with transfer matrices of an elastic and an air layer. The reduction to the total velocity and the total stress of a poroelastic layer can be performed by applying the permeability condition at the surface of a poroelastic layer.

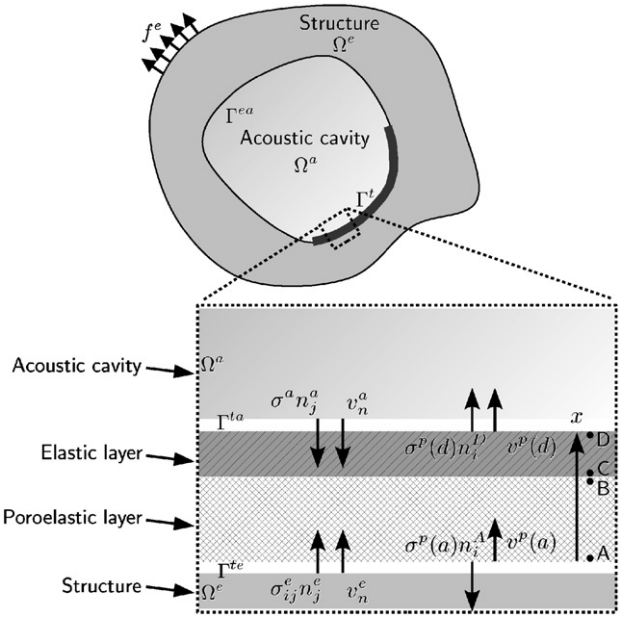

Fig. 2. Two-layered structure, located on the coupling surface between the structure and the acoustic cavity, consisting of a poroelastic layer glued to an elastic layer.

When the surface of a poroelastic layer is not permeable, the velocity v^s of the solid phase is equal to that of the fluid phase at the surface. Assuming the continuity of velocity and stress at the surface, v^p and σ^p satisfy the following relations:

$$\begin{aligned} v^s(x) - v^f(x) &= 0, \\ v^s(x) &= v^p(x), \\ \sigma^s(x) + \sigma^f(x) &= \sigma^p(x). \end{aligned} \tag{31}$$

When the surface is permeable, v^p and σ^p satisfy the following relations owing to the continuity of pressure, volume velocity and stress at the surface:

$$\phi\sigma^s(x) - (1-\phi)\sigma^f(x) = 0,$$

$$(1-\phi)v^s(x) + \phi v^f(x) = v^p(x),$$

$$\sigma^s(x) + \sigma^f(x) = \sigma^p(x). \tag{32}$$

The relations (31) and (32) can be rewritten as

$$\mathbf{H}\mathbf{V}(x) = \mathbf{V}^p(x), \tag{33}$$

where

$$\mathbf{V}^p(x) = [0 \; v^p(x) \; \sigma^p(x)]^{\mathrm{T}}. \tag{34}$$

$\mathbf{H}$ is defined according to the permeability of a poroelastic layer surface. For an impermeable surface,

$$\mathbf{H} = \begin{bmatrix} 1 & -1 & 0 & 0 \\ 1 & 0 & 0 & 0 \\ 0 & 0 & 1 & 1 \end{bmatrix}, \tag{35}$$

and for a permeable surface,

$$\mathbf{H} = \begin{bmatrix} 0 & 0 & \phi & -(1-\phi) \\ 1-\phi & \phi & 0 & 0 \\ 0 & 0 & 1 & 1 \end{bmatrix}. \tag{36}$$

If $\mathbf{H}$ is equal to $\mathbf{H}_A$ for the surface at $x = a$, and $\mathbf{H}_B$ for the surface at $x = b$, then we can obtain the following relations:

$$\mathbf{H}_A\mathbf{V}(a) = \mathbf{V}^p(a), \tag{37}$$

$$\mathbf{H}_B\mathbf{V}(b) = \mathbf{V}^p(b). \tag{38}$$

From Eqs. (29), (37), and (38), $v^p(a)$ and $\sigma^p(a)$ are related to $v^p(b)$ and $\sigma^p(b)$ by

$$\begin{bmatrix} v^p(a) \\ \sigma^p(a) \end{bmatrix} = \mathbf{T}_{AB} \begin{bmatrix} v^p(b) \\ \sigma^p(b) \end{bmatrix}, \tag{39}$$

where $\mathbf{T}_{AB}$ is the reduced transfer matrix of a poroelastic layer whose size is 2×2. The reduced transfer matrix $\mathbf{T}_{AB}$ can be multiplied with transfer matrices of other media such as elastic media or acoustic media since they have the same dimension. Moreover, we can implement the reduced transfer matrix for boundary conditions at the coupling surface between a structure and an acoustic cavity.

2.4. Implementation of reduced transfer matrix in coupled problem

In this section, we implement the reduced transfer matrix as boundary conditions at the coupling surface in the structural–acoustic coupled problem, supposing that the wave propagation in a multilayered structure along the direction normal to the coupling surface is dominant. Now we consider only the continuity of the

velocity and the stress normal to the coupling surface. The continuity of the velocity and the stress at point A ($x = a$) and point D ($x = d$) in Fig. 2 gives the following boundary conditions:

$$\begin{bmatrix} v_n^e \\ \sigma_{ij}^e n_j^e \end{bmatrix} = -\begin{bmatrix} -1 & 0 \\ 0 & n_i^A \end{bmatrix} \begin{bmatrix} v^p(a) \\ \sigma^p(a) \end{bmatrix}, \tag{40}$$

$$\begin{bmatrix} v_n^a \\ \sigma^a n_i^a \end{bmatrix} = -\begin{bmatrix} 1 & 0 \\ 0 & n_i^D \end{bmatrix} \begin{bmatrix} v^p(d) \\ \sigma^p(d) \end{bmatrix}, \tag{41}$$

where v_n^e and v_n^a are the normal velocities, σ_{ij}^e and σ^a are the stresses for the structural and the acoustic domain at the coupling surface as shown in Fig. 2; n_i^e and n_i^a are the unit normal vectors for the structural–acoustic coupling surface; n_i^A and n_i^D are, respectively, the unit normal vectors pointing outward at point A and point D. The total velocity $v^p(a)$ and the total stress $\sigma^p(a)$ at point A are related to $v^p(d)$ and $\sigma^p(d)$ at point D by

$$\begin{bmatrix} v^p(a) \\ \sigma^p(a) \end{bmatrix} = \mathbf{T}_{AD} \begin{bmatrix} v^p(d) \\ \sigma^p(d) \end{bmatrix}, \tag{42}$$

where $\mathbf{T}_{AD}$ is the reduced transfer matrix of the size 2×2 between point A and point D given by

$$\mathbf{T}_{AD} = \begin{bmatrix} t_{11} & t_{12} \\ t_{21} & t_{22} \end{bmatrix}. \tag{43}$$

Applying the reciprocity of a multilayered structure that gives $|\mathbf{T}_{AD}| = 1$, the boundary conditions (40) and (41) can be rewritten as

$$v_n^a = -\frac{1}{t_{11}} v_n^e + \frac{t_{12}}{t_{11}} \mathrm{j}\omega\phi^a, \tag{44}$$

$$\sigma_{ij}^e n_j^e = \frac{t_{21}}{t_{11}} v_n^e n_i^e + \frac{1}{t_{11}} \mathrm{j}\omega\phi^a n_i^e, \tag{45}$$

where ϕ^a is the potential of an acoustic domain defined as $\sigma^a = \mathrm{j}\omega\phi^a$. Eqs. (44) and (45) are regarded as the boundary conditions for the structural–acoustic coupled problem having a multilayered structure. The weak formulations of the coupled problem become

$$\begin{aligned} &\int_{\Omega^e} (\sigma_{ij}^e \delta\varepsilon_{ij}^e - \rho^e \omega^2 u_i^e \delta u_i^e)\, \mathrm{d}\Omega - \int_{\Gamma^{ea}} \mathrm{j}\omega\phi^a \delta u_n^e \, \mathrm{d}\Gamma \\ &\quad - \int_{\Gamma^t} \frac{1}{t_{11}} \mathrm{j}\omega\phi^a \delta u_n^e \, \mathrm{d}\Gamma - \int_{\Gamma^t} \frac{t_{21}}{t_{11}} \mathrm{j}\omega u_n^e \delta u_n^e \, \mathrm{d}\Gamma = \int_{\Gamma^f} f_i^e \delta u_i^e \, \mathrm{d}\Gamma, \end{aligned} \tag{46}$$

$$\begin{aligned} &\int_{\Omega^a} \left(-\frac{1}{\rho^a} \frac{\partial\phi^a}{\partial x_i} \frac{\partial\delta\phi^a}{\partial x_i} + \frac{\omega^2}{\rho^a c^2} \phi^a \delta\phi^a \right) \mathrm{d}\Omega - \int_{\Gamma^{ea}} \mathrm{j}\omega u_n^e \delta\phi^a \, \mathrm{d}\Gamma \\ &\quad - \int_{\Gamma^t} \frac{1}{t_{11}} \mathrm{j}\omega u_n^e \delta\phi^a \, \mathrm{d}\Gamma + \int_{\Gamma^t} \frac{t_{12}}{t_{11}} \mathrm{j}\omega\phi^a \delta\phi^a \, \mathrm{d}\Gamma = 0, \end{aligned} \tag{47}$$

where ε_{ij}^e is the strain of a structural domain, ρ^e and ρ^a, respectively, the densities of a structural and an acoustic domain, c the speed of sound in an acoustic domain, and f^e the external load applied to the boundary Γ^f of a structural domain.

When the standard finite element procedure is applied, we obtain the equilibrium equation written as

$$\left\{ \begin{bmatrix} \mathbf{K}_e & \mathbf{O} \\ \mathbf{O} & \mathbf{K}_a \end{bmatrix} - \omega^2 \begin{bmatrix} \mathbf{M}_e & \mathbf{O} \\ \mathbf{O} & \mathbf{M}_a \end{bmatrix} - \mathrm{j}\omega \begin{bmatrix} \mathbf{O} & \mathbf{C} \\ \mathbf{C}^{\mathrm{T}} & \mathbf{O} \end{bmatrix} - \mathrm{j}\omega \begin{bmatrix} \mathbf{C}_2 & \mathbf{C}_1 \\ \mathbf{C}_1^{\mathrm{T}} & \mathbf{C}_3 \end{bmatrix} \right\} \begin{bmatrix} \mathbf{U}_e \\ \mathbf{\Phi}_a \end{bmatrix} = \begin{bmatrix} \mathbf{F}_e \\ \mathbf{O} \end{bmatrix}, \tag{48}$$

where $\mathbf{K}_e$ and $\mathbf{K}_a$ are the stiffness matrices for a structure and an acoustic cavity, $\mathbf{M}_e$ and $\mathbf{M}_a$ the mass matrices for a structure and an acoustic cavity, $\mathbf{C}$ the coupling matrix for the coupling surface without a multilayered structure, $\mathbf{U}_e$ the displacement vector of a structure, $\mathbf{\Phi}_a$ the velocity potential vector of an acoustic cavity, and

$\mathbf{F}_e$ the external load vector. For the coupling surface with a multilayered structure, the coupling matrix $\mathbf{C}_1$, the structural impedance matrix $\mathbf{C}_2$, and the acoustic impedance matrix $\mathbf{C}_3$ are derived as

$$\mathbf{C}_1 = \sum_{i=1}^{n_t} \int_{\Gamma_i^t} \frac{1}{t_{11}} \mathbf{N}_e^{\mathrm{T}} \mathbf{n}_e \mathbf{N}_a \, \mathrm{d}\Gamma, \tag{49}$$

$$\mathbf{C}_2 = \sum_{i=1}^{n_t} \int_{\Gamma_i^t} \frac{t_{21}}{t_{11}} \mathbf{N}_e^{\mathrm{T}} \mathbf{n}_e \mathbf{n}_e^{\mathrm{T}} \mathbf{N}_e \, \mathrm{d}\Gamma, \tag{50}$$

$$\mathbf{C}_3 = \sum_{i=1}^{n_t} \int_{\Gamma_i^t} -\frac{t_{12}}{t_{11}} \mathbf{N}_a^{\mathrm{T}} \mathbf{N}_a \, \mathrm{d}\Gamma, \tag{51}$$

where $\mathbf{N}_e$ and $\mathbf{N}_a$ are, respectively, the shape function matrices for a structure and an acoustic cavity, $\mathbf{n}_e$ is the unit normal vector on the structural surface, and n_t is the number of elements on the coupling surface with a multilayered structure Γ^t.

In Eq. (48), one can find that the matrix consisting of $\mathbf{C}_1$, $\mathbf{C}_2$, and $\mathbf{C}_3$ is appended to the standard equilibrium equation of the structural–acoustic coupled problem without a multilayered structure. The direct approach has to be applied to obtain frequency responses since the coefficients t_{ij} in $\mathbf{C}_1$, $\mathbf{C}_2$, and $\mathbf{C}_3$ are dependent on frequencies. If a multilayered structure does not cause the significant change of eigenmodes of a structure and an acoustic cavity, then responses can be approximately calculated via the modal approach, utilizing uncoupled structural and acoustic eigenmodes. This enables considerable computational cost savings.

3. Thickness optimization of multilayered structures

3.1. Formulation of optimization problem

To fulfill the requirements of reducing both the weight of a multilayered structure and sound pressure levels inside an acoustic cavity, we consider the optimization problem of minimizing sound pressure levels under the volume constraint of a multilayered structure. Let $\mathbf{x}$ be the position vector at the coupling surface with a multilayered structure Γ^t. In this study, the thickness of a poroelastic layer $t(\mathbf{x})$ is regarded as design variables while the thickness of an elastic layer is held constant. Note that thicknesses for arbitrary number of layers in a multilayered structure can be regarded as design variables in the same way as what is described below.

Since the papers by Cheng and Olhoff [1], it has been by now well known that, in the thickness optimization problems of elastic plates, the optimal plate includes the infinite number of the infinitely thin stiffeners with the extreme discontinuities of the thickness distribution. Considering this fact, we can assume that the optimal thickness of a poroelastic layer $t(\mathbf{x})$ may also include the extreme discontinuities although it has not been demonstrated yet. In order to make the problem well-posed, some regularization or smoothing technique should be introduced. Based on the key idea of the density approach in topology optimization, the thickness of a poroelastic layer $t(\mathbf{x})$ is expressed in a relaxed form as

$$t(\mathbf{x}) = \mu^p(\mathbf{x}) t_{\max}, \tag{52}$$

where $\mu(\mathbf{x})$ is a density function with C^0 continuity ranging between 0 and 1, p is the penalization parameter, and $t_{\max}$ denotes the prescribed maximum thickness of the poroelastic layer. Volume m of the poroelastic layer is written as

$$m = \int_{\Gamma^t} \mu(\mathbf{x}) t_{\max} \, \mathrm{d}\Gamma. \tag{53}$$

In topology optimization problems, the penalization parameter p equal to or larger than 3 is mostly applied in order to penalize intermediate values of $\mu(\mathbf{x})$ and reduce effectively grey scale areas (see, e.g., Ref. [31]). However, in thickness optimization problems, intermediate values can be physically realized and equally acceptable. Therefore, the penalization parameter p is assigned the value 1 in this paper.

For the objective function F, we here define the mean squared sound pressure level within the prescribed frequency range $f_1 \leqslant f \leqslant f_2$ over the partial domain Ω^c of the acoustic domain Ω^a. Considering the relation $p^a = -\mathrm{j}\omega\phi^a$, the objective function F is written as

$$F = \int_{\omega_1}^{\omega_2} \left(\int_{\Omega^c} \omega^2 \phi^a \phi^{a*} \, \mathrm{d}\Omega \right) \mathrm{d}\omega, \tag{54}$$

where $\omega_1 = 2\pi f_1$ and $\omega_2 = 2\pi f_2$, and * denotes complex conjugate. Introducing the spectrum of the objective function F_ω written as $F_\omega = \int_{\Omega^c} \omega^2 \phi^a \phi^{a*} \, \mathrm{d}\Omega$, and regarding the density function $\mu(\mathbf{x})$ as design variables, the optimization problem can be defined as

$$\begin{aligned} \underset{\mu}{\text{minimize}} \quad & F = \int_{\omega_1}^{\omega_2} F_\omega \, \mathrm{d}\omega \\ \text{subject to} \quad & m - m_0 \leqslant 0, \\ & \text{equilibrium equations (46), (47),} \\ & 0 < \mu(\mathbf{x}) \leqslant 1, \end{aligned} \tag{55}$$

where m_0 is the upper bound for the volume of the poroelastic layer.

3.2. Continuous approximation

The optimization problem (55) is usually solved numerically utilizing discretized design variables in conjunction with the FEM to solve equilibrium equations. Considering the relaxed form of thickness in Eq. (52), thickness should be distributed continuously over the design domain, and this status must hold even after discretization of the thickness distribution. If the discretized design variables are assigned in elements for the FEM, they are usually set to piecewise constants within an element. Therefore, a sufficiently fine mesh is required to be consistent with the continuous thickness distribution in Eq. (52). Unfortunately, using such a fine mesh places severe demands upon calculation resources.

To overcome the problem, we assume the continuous approximation of material distribution proposed by Matsui and Terada [14] and Rahmatalla and Swan [15]. This means the design variable $\mu(\mathbf{x})$ is assumed to be continuous over the design domain. The discretized design variables μ_i are assigned at nodes of elements, and we approximate the design variable $\mu(\mathbf{x})$ as

$$\mu(\mathbf{x}) \simeq \mathbf{N}_t^{\mathrm{T}} \boldsymbol{\mu} = \sum_{i=1}^{n_d} N_{ti} \mu_i, \tag{56}$$

where $\mathbf{N}_t$ is a vector whose components N_{ti} are interpolation functions, $\boldsymbol{\mu}$ is a vector of the discretized nodal design variables μ_i, and n_d is the number of design variables. The bilinear interpolation function is here used as N_{ti} in the case where quadrilateral elements are applied for its simplicity. Thus, the design variable $\mu(\mathbf{x})$ can hold C^0 continuity throughout the design domain due to the partition-of-unity property even after the discretization.

Applying the finite element discretization with the continuous approximation of design variables in Eq. (56), the optimization problem can be formulated as

$$\begin{aligned} \underset{\mu_i}{\text{minimize}} \quad & F = \int_{\omega_1}^{\omega_2} F_\omega \, \mathrm{d}\omega \\ \text{subject to} \quad & m - m_0 \leqslant 0, \\ & \mathbf{D} \begin{bmatrix} \mathbf{U}_e \\ \boldsymbol{\Phi}_a \end{bmatrix} - \begin{bmatrix} \mathbf{F}_e \\ \mathbf{O} \end{bmatrix} = \mathbf{O}, \\ & 0 < \mu_{\min} \leqslant \mu_i \leqslant 1 \quad (i = 1, 2, \ldots, n_d), \end{aligned} \tag{57}$$

where

$$F_\omega = \sum_{i=1}^{n_e} \int_{\Omega_i^e} \omega^2 \boldsymbol{\Phi}_a^{\mathrm{T}} \mathbf{N}_a^{\mathrm{T}} \mathbf{N}_a \boldsymbol{\Phi}_a^* \, \mathrm{d}\Omega, \tag{58}$$

$$m = \sum_{i=1}^{n_t} \int_{\Gamma_i^t} \mathbf{N}_t^{\mathrm{T}} \boldsymbol{\mu} t_{\max} \, \mathrm{d}\Gamma, \tag{59}$$

$$\mathbf{D} = \left\{ \begin{bmatrix} \mathbf{K}_e & \mathbf{O} \\ \mathbf{O} & \mathbf{K}_a \end{bmatrix} - \omega^2 \begin{bmatrix} \mathbf{M}_e & \mathbf{O} \\ \mathbf{O} & \mathbf{M}_a \end{bmatrix} - \mathrm{j}\omega \begin{bmatrix} \mathbf{O} & \mathbf{C} \\ \mathbf{C}^{\mathrm{T}} & \mathbf{O} \end{bmatrix} - \mathrm{j}\omega \begin{bmatrix} \mathbf{C}_2 & \mathbf{C}_1 \\ \mathbf{C}_1^{\mathrm{T}} & \mathbf{C}_3 \end{bmatrix} \right\}. \tag{60}$$

$\mathbf{D}$ is the dynamic stiffness matrix; n_c and n_t are, respectively, the number of elements in the domain Ω^c and the boundary Γ^t; $\mu_{\min}$ is a lower bound of design variables μ_i.

3.3. Optimization algorithm

The optimization algorithm to solve the problem defined in Eq. (57) is explained through the flowchart shown in Fig. 3 consisting of five steps in an iteration loop. In the first step, the transfer matrix of the multilayered structure is calculated using design variables. In the second step, the equilibrium equations of the system are solved. In the third step, the objective function and the volume of the poroelastic layer are calculated. If the objective function is converged, the optimal thickness distribution is obtained. Otherwise, the sensitivities of the objective function and the volume constraint with respect to the design variables are computed in the fourth step. In the final step, design variables are updated using SLP (Sequential Linear Programming). These procedures are iterated until the objective function reaches convergence.

3.4. Design sensitivity analysis

Design sensitivities of objective functions and constraints with respect to design variables are required for updating of design variables using SLP. The sensitivities can be calculated rather quickly by adopting the adjoint variable method. The adjoint variables $\mathbf{V}_e$ and $\boldsymbol{\Psi}_a$ are now introduced for the structural displacement and the acoustic potential, respectively. Since the equilibrium equation (48) is satisfied, the spectrum of the objective function F_ω is equal to L_ω which is defined as

$$L_\omega = F_\omega + [\mathbf{V}_e^{\mathrm{T}} \ \boldsymbol{\Psi}_a^{\mathrm{T}}] \left\{ \begin{bmatrix} \mathbf{F}_e \\ \mathbf{O} \end{bmatrix} - \mathbf{D} \begin{bmatrix} \mathbf{U}_e \\ \boldsymbol{\Phi}_a \end{bmatrix} \right\} + [\mathbf{V}_e^{*\mathrm{T}} \ \boldsymbol{\Psi}_a^{*\mathrm{T}}] \left\{ \begin{bmatrix} \mathbf{F}_e^* \\ \mathbf{O} \end{bmatrix} - \mathbf{D}^* \begin{bmatrix} \mathbf{U}_e^* \\ \boldsymbol{\Phi}_a^* \end{bmatrix} \right\}. \tag{61}$$

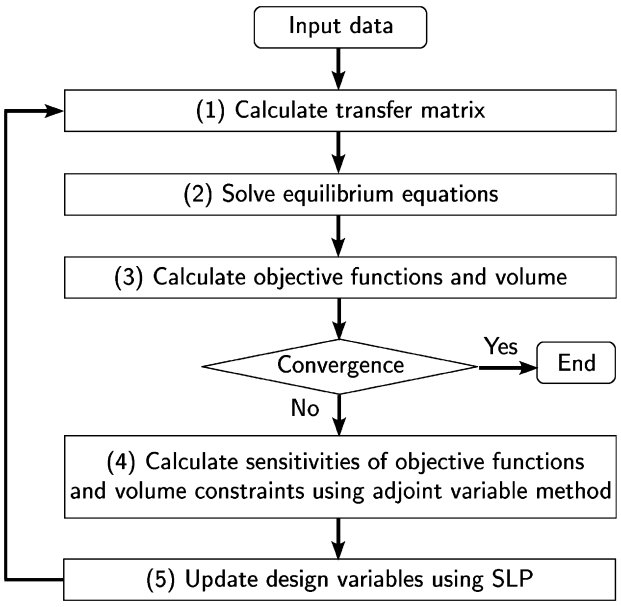

Fig. 3. Flowchart of the optimization procedure.

Supposing that the external load $\mathbf{F}_e$ is independent of design variables μ_i, the derivative of L_ω with respect to design variables μ_i can be written as

$$\frac{\mathrm{d}L_\omega}{\mathrm{d}\mu_i} = -[\mathbf{V}_e^{\mathrm{T}} \ \ \boldsymbol{\Psi}_a^{\mathrm{T}}]\frac{\partial \mathbf{D}}{\partial \mu_i}\begin{bmatrix}\mathbf{U}_e\\ \boldsymbol{\Phi}_a\end{bmatrix} - [\mathbf{V}_e^{*\mathrm{T}} \ \ \boldsymbol{\Psi}_a^{*\mathrm{T}}]\frac{\partial \mathbf{D}^*}{\partial \mu_i}\begin{bmatrix}\mathbf{U}_e^*\\ \boldsymbol{\Phi}_a^*\end{bmatrix} + \left\{\begin{bmatrix}\mathbf{O} & \dfrac{\partial F_\omega}{\partial \boldsymbol{\Phi}_a}\end{bmatrix} - [\mathbf{V}_e^{\mathrm{T}} \ \ \boldsymbol{\Phi}_a^{\mathrm{T}}]\mathbf{D}\right\}\begin{bmatrix}\dfrac{\partial \mathbf{U}_e}{\partial \mu_i}\\ \dfrac{\partial \boldsymbol{\Phi}_a}{\partial \mu_i}\end{bmatrix} + \left\{\begin{bmatrix}\mathbf{O} & \dfrac{\partial F_\omega}{\partial \boldsymbol{\Phi}_a^*}\end{bmatrix} - [\mathbf{V}_e^{*\mathrm{T}} \ \ \boldsymbol{\Psi}_a^{*\mathrm{T}}]\mathbf{D}^*\right\}\begin{bmatrix}\dfrac{\partial \mathbf{U}_e^*}{\partial \mu_i}\\ \dfrac{\partial \boldsymbol{\Psi}_a^*}{\partial \mu_i}\end{bmatrix}. \tag{62}$$

Therefore we can define the adjoint equation such that

$$\mathbf{D}\begin{bmatrix}\mathbf{V}_e\\ \boldsymbol{\Psi}_a\end{bmatrix} - \begin{bmatrix}\mathbf{O}\\ \dfrac{\partial F_\omega}{\partial \boldsymbol{\Phi}_a}\end{bmatrix} = \mathbf{O}. \tag{63}$$

Substituting the solutions $\mathbf{V}_e$ and $\boldsymbol{\Psi}_a$ for the adjoint equation (63) into Eq. (62), we derive the derivative of the objective function F with respect to design variables μ_i:

$$\frac{\mathrm{d}F}{\mathrm{d}\mu_i} = \int_{\omega_1}^{\omega_2}\left(-[\mathbf{V}_e^{\mathrm{T}} \ \ \boldsymbol{\Psi}_a^{\mathrm{T}}]\frac{\partial \mathbf{D}}{\partial \mu_i}\begin{bmatrix}\mathbf{U}_e\\ \boldsymbol{\Phi}_a\end{bmatrix} - [\mathbf{V}_e^{*\mathrm{T}} \ \ \boldsymbol{\Psi}_a^{*\mathrm{T}}]\frac{\partial \mathbf{D}^*}{\partial \mu_i}\begin{bmatrix}\mathbf{U}_e^*\\ \boldsymbol{\Phi}_a^*\end{bmatrix}\right)\mathrm{d}\omega. \tag{64}$$

By the chain rule, the derivative of the dynamic stiffness matrix $\mathbf{D}$ with respect to design variables μ_i is written as

$$\frac{\partial \mathbf{D}}{\partial \mu_i} = -\mathrm{j}\omega p \mu_i^{p-1} t_{\max}\frac{\partial}{\partial t_i}\begin{bmatrix}\mathbf{C}_2 & \mathbf{C}_1\\ \mathbf{C}_1^{\mathrm{T}} & \mathbf{C}_3\end{bmatrix}. \tag{65}$$

The derivatives of the coupling matrix $\mathbf{C}_1$ and the impedance matrix $\mathbf{C}_2$, $\mathbf{C}_3$ with respect to the thickness t_i are given by

$$\frac{\partial \mathbf{C}_1}{\partial t_i} = \sum_{j=1}^{n_t}\int_{\Gamma_j^t}\frac{-t'_{11}}{t_{11}^2}\mathbf{N}_e^{\mathrm{T}}\mathbf{n}_e\mathbf{N}_a\,\mathrm{d}\Gamma, \tag{66}$$

$$\frac{\partial \mathbf{C}_2}{\partial t_i} = \sum_{j=1}^{n_t}\int_{\Gamma_j^t}\frac{t'_{21}t_{11} - t_{21}t'_{11}}{t_{11}^2}\mathbf{N}_e^{\mathrm{T}}\mathbf{n}_e\mathbf{n}_e^{\mathrm{T}}\mathbf{N}_e\,\mathrm{d}\Gamma, \tag{67}$$

$$\frac{\partial \mathbf{C}_3}{\partial t_i} = \sum_{j=1}^{n_t}\int_{\Gamma_j^t}-\frac{t'_{12}t_{11} - t_{12}t'_{11}}{t_{11}^2}\mathbf{N}_a^{\mathrm{T}}\mathbf{N}_a\,\mathrm{d}\Gamma, \tag{68}$$

where t'_{11}, t'_{12}, and t'_{21} denote the derivatives of t_{11}, t_{12}, and t_{21} with respect to the thickness t_i, respectively.

The derivative of volume of the poroelastic layer m with respect to design variables μ_i is easily derived as

$$\frac{\partial m}{\partial \mu_i} = \sum_{i=1}^{n_t}\int_{\Gamma_i^t}\mathbf{N}_t^{\mathrm{T}}\boldsymbol{\delta}_i t_{\max}\,\mathrm{d}\Gamma, \tag{69}$$

where $\boldsymbol{\delta}_i$ is the vector having unity in the row corresponding to μ_i and zeros elsewhere.

4. Numerical examples

As illustrated in Fig. 4, a flat steel panel coupled with a multilayered structure and an acoustic cavity is applied for numerical confirmation examples. The panel is 0.365 m long, 0.250 m wide, and 0.0012 m thick, and is supported along all edges. The acoustic cavity has the same length and width as the panel, and has 0.490 m height. The bottom surface of the cavity is coupled with the multilayered structure and the other

surfaces are assumed to have rigid boundaries. An external unit point load is enforced at the center of the panel. The multilayered structure located between the panel and the cavity consists of a poroelastic layer 0.030 m thick and an elastic layer 0.002 m thick. The poroelastic layer is glued to the elastic layer, but not glued to the panel.

The steel panel has Young's modulus of 2.10×10^{11} Pa, the loss factor of zero, the density of 7860 kg m^{-3}, and Poisson's ratio of 0.29. In the acoustic cavity, the speed of sound is 340 m s^{-1} and the density of the air contained in is 1.225 kg m^{-3}. The material properties of the poroelastic layer are listed in Table 1 for the solid phase and in Table 2 for the fluid phase. The material properties of the elastic layer are also listed in Table 1.

4.1. Transfer matrix representation

First of all, the transfer matrix representation of a multilayered structure located between a structure and an acoustic cavity is verified by comparing this with a finite element representation in terms of accuracy and computational costs. For the finite element representation, the multilayered structure is also modeled by finite

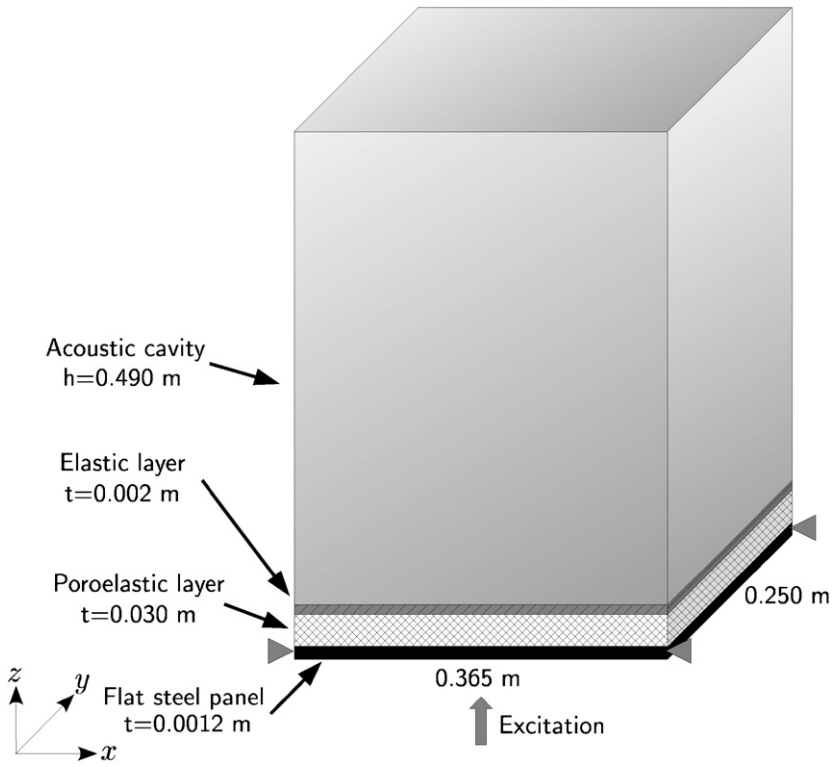

Fig. 4. A schematic view of example model.

Table 1
Structural parameters of the materials used in the multilayered structure

Structural parameters			Poroelastic layer	Elastic layer
Young's modulus	E	Pa	2.67×10^5	1.75×10^8
Loss factor	η	–	0.11	0.25
Density	ρ	kg m^{-3}	43	1787
Poisson's ratio	ν	–	0.4	0.4

Table 2
Acoustic parameters of the material used in the multilayered structure

Acoustic parameters			Poroelastic layer
Porosity	ϕ	–	0.97
Tortuosity	α_∞	–	2.5
Flow resistivity	σ	$\mathrm{N\,s\,m^{-4}}$	7.0×10^{4}
Viscous characteristic length	Λ	m	3.6×10^{-5}
Thermal characteristic length	Λ'	m	1.69×10^{-4}

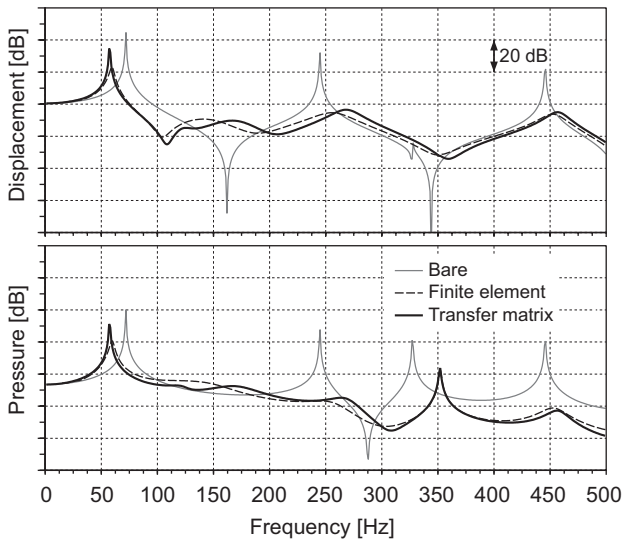

Fig. 5. Frequency response of displacement of the panel (upper) and pressure in the cavity (lower) when the poroelastic layer is not glued to the panel: response using the finite element representation (solid line), response using transfer matrix representation (dashed line), and the reference response when the multilayered structure is removed (solid grey line).

elements, and the analysis model has 48,877 degrees of freedom. To obtain frequency responses, the direct solution is applied here.

Fig. 5 shows the frequency responses of the z displacement at the center of the panel and the pressure at the center of the top surface of the acoustic cavity when the multilayered structure is not glued to the panel. The solid line gives the response calculated by the finite element representation; the dashed line shows the response calculated by the transfer matrix representation. The solid grey line shows a reference response when the multilayered structure is removed.

The peaks observed at 70, 245, and 440 Hz are caused by the resonance characteristics of the flat steel panel, and the peak at 340 Hz by the resonance of the acoustic cavity. Though there are some discrepancies between the response by the finite element representation and that by the transfer matrix representation in the neighborhood of 150 Hz, good agreements are generally obtained through the entire frequency range.

Fig. 6 shows the responses when the multilayered structure is glued to the panel. Here, the response given by the transfer matrix representation is not consistent with the response by the finite element representation since the shear wave in the poroelastic medium, which is not taken into account in the transfer matrix representation, has an impact on the response. In this case, the multilayered structure must be modeled including the shear wave using, for instance, the finite element representation.

In terms of computational costs, approximately 44,000 s were required to calculate responses at 500 frequency lines applying the finite element representation and the direct solution. In contrast, only approximately 180 s were required to calculate the eigenmodes, and only 6 s were required to calculate responses at 500 frequency lines applying the transfer matrix representation and the modal solution. Note that

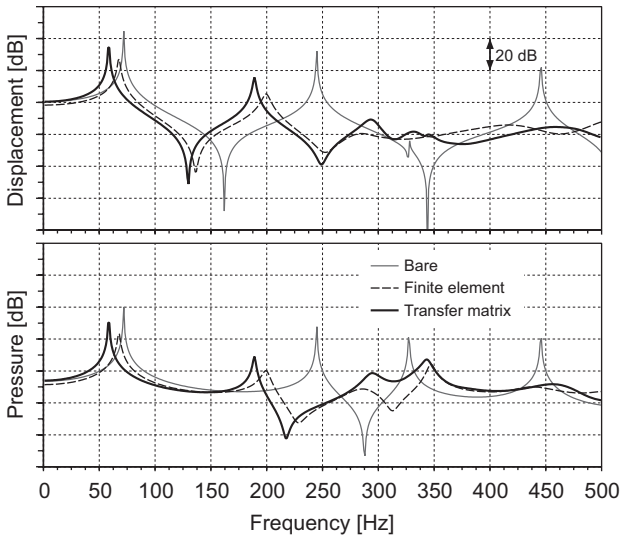

Fig. 6. Frequency response of displacement of the panel (upper) and pressure in the cavity (lower) when the poroelastic layer is glued to the panel: response using the finite element representation (solid line), response using transfer matrix representation (dashed line), and the reference response when the multilayered structure is removed (solid grey line).

the computation is carried out on IBM 7039-651 in this example. Thus, the latter method appears capable of reducing computational demands by a factor that approaches 200, while preserving practical accuracy. This process is extremely efficient with respect to iterative calculations required in optimization process.

4.2. Frequency ranges to be optimized

Here we regard the whole domain of the acoustic cavity Ω^a as the evaluation domain Ω^e subject to be optimized in order to obtain the optimal thickness distribution independent of the definition of the domain Ω^e.

Fig. 7 shows the spectrum of the objective function F_ω for the initial uniform thickness of the multilayered structure as drawn in Fig. 8. One can see peaks of the spectrum around 250 and 450 Hz when the multilayered structure is removed. The peaks are rather well damped by the multilayered structure laid on the panel, but the peak due to the resonance of the panel around 55 Hz, and the peak due to the resonance of the acoustic cavity around 350 Hz still show high spectrum levels. In this example, the frequency range from 45 to 70 Hz including the resonance of the panel around 55 Hz, and the frequency range from 340 to 365 Hz including the resonance of the cavity around 350 Hz, are chosen to be minimized by the optimization method proposed in Section 3.

The discretized thicknesses of the poroelastic layer are regarded as design variables while the thickness of the elastic layer is held constant. The number of design variables is equal to the number of nodes on the coupling surface, 999. The upper bound $t_{\max}$ of the thickness of the poroelastic layer is set to 0.090 m and the initial uniform thickness is assumed to be 0.030 m which corresponds to the initial design variables $\rho_i = 0.333$. The lower bound $\mu_{\min}$ of design variables is set to 0.01. The volume for the initial uniform thickness of the poroelastic layer is used as the upper bound m_0 for the volume of the poroelastic layer.

4.3. Frequency range 1

The results of the optimization for the frequency range from $f_1 = 45$ Hz to $f_2 = 70$ Hz are described in this section. Fig. 9 shows the iteration history for the objective function and for the volume that are normalized to the initial quantities. The value of the objective function decreases significantly to less than 3%, while the volume remains 100% during the iterations.

The optimal thickness distribution is shown in Fig. 10, and we observe that the thickness near the center is at the maximum ($\mu_i = 1.0$) whereas near the edge, it becomes very small ($\mu_i \simeq 0.016$).

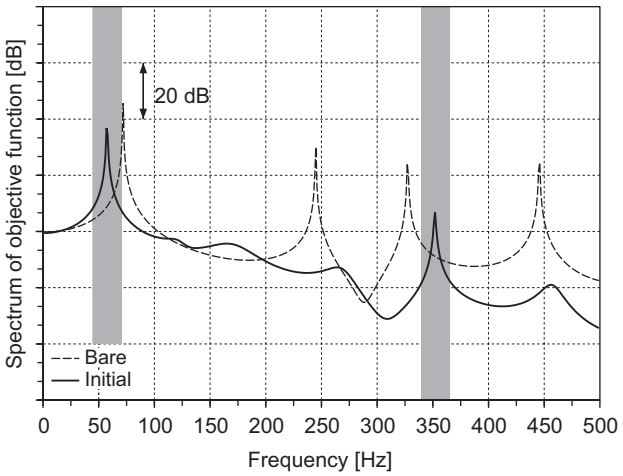

Fig. 7. Spectrum of objective function for the initial thickness (solid line) and reference spectrum when the multilayered structure is removed (dashed line). Target frequency ranges including a spectrum peak to be minimized are highlighted. The first covers from 45 to 70 Hz; the second from 340 to 365 Hz.

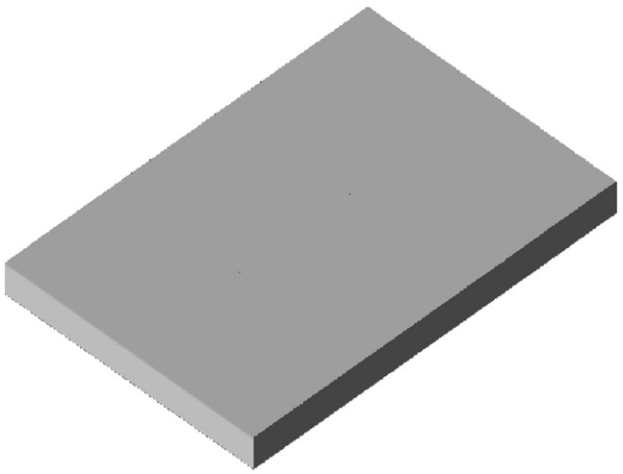

Fig. 8. Initial uniform thickness distribution of poroelastic layer.

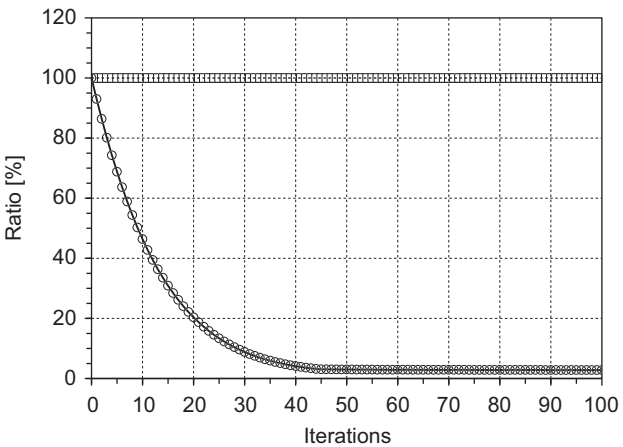

Fig. 9. Iteration histories of objective function (circle) and volume (square) for the optimization in the frequency range from 45 to 70 Hz.

Fig. 11 offers the comparison between the response for the initial uniform thickness and that for the optimal thickness distribution, and shows the frequency response of the displacement at the center of the panel and the sound pressure level at the center of the top surface of the cavity. In the frequency range from 45 to 70 Hz subject to the optimization, the displacement of the panel is rather damped by the optimal thickness distribution, and the sound pressure level in the cavity has decreased significantly. However, the sound pressure level over 200 Hz, where the optimization scheme does not apply, has increased.

Fig. 12 shows the frequency responses for the initial and the optimal thickness distribution obtained using the finite element method, where the multilayered structure is represented by finite volume elements. The responses are calculated at the same positions as those in Fig. 11. We can see that the sound pressure level in the target frequency range from 45 to 70 Hz has decreased considerably, although the absolute degree of the reduction in the sound pressure level does not agree to that in Fig. 11.

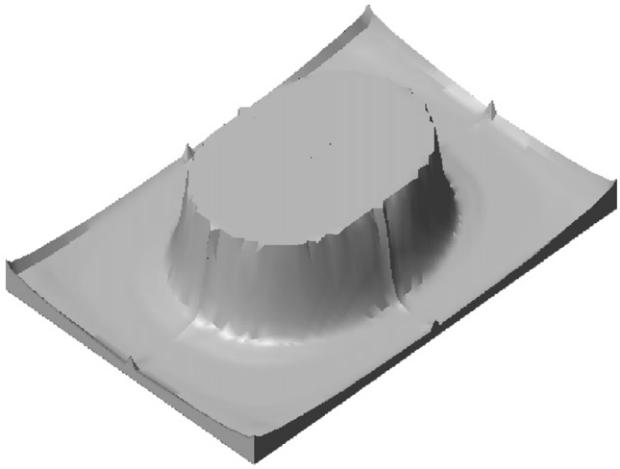

Fig. 10. Optimal thickness distribution for the optimization in the frequency range from 45 to 70 Hz.

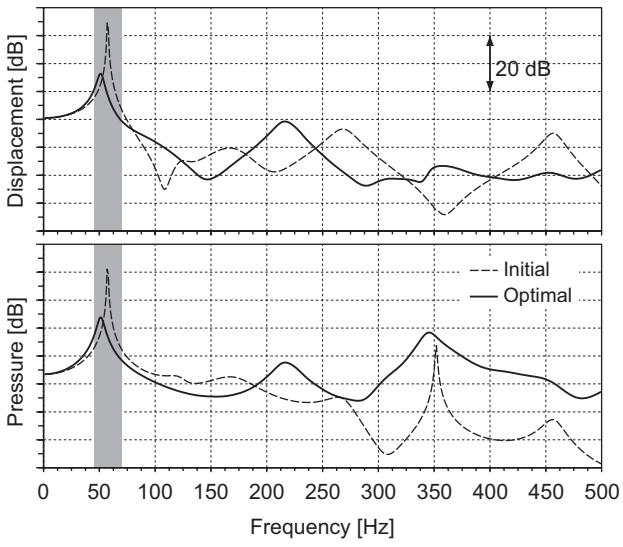

Fig. 11. Frequency response of displacement of the panel (upper) and pressure in the cavity (lower). Dashed line shows the initial uniform thickness and solid line shows the optimal thickness distribution for the frequency range of 45–70 Hz.

4.4. Frequency range 2

The results of the optimization for the frequency range from $f_1 = 340$ Hz to $f_2 = 365$ Hz are explained next. Fig. 13 shows the iteration history for the objective function and the volume of the poroelastic layer. Both the objective function and the volume decrease in this case.

The optimal thickness distribution is illustrated in Fig. 14. It appears that design variables across most of the design domain have become smaller ($\mu_i = 0.20$–0.34) in comparison with the initial design variables, $\mu_i = 0.333$.

Fig. 15 shows the frequency response of the displacement at the center of the panel and the sound pressure level at the center of the cavity's top surface. The sound pressure level in the frequency range from 340 to 365 Hz subject to the optimization has decreased, while the level of panel displacement is almost unaffected.

Fig. 16 shows the frequency responses obtained using the finite element approach, where the multilayered structure is also discretized by finite volume elements. We can see that the impact of the reduction on the

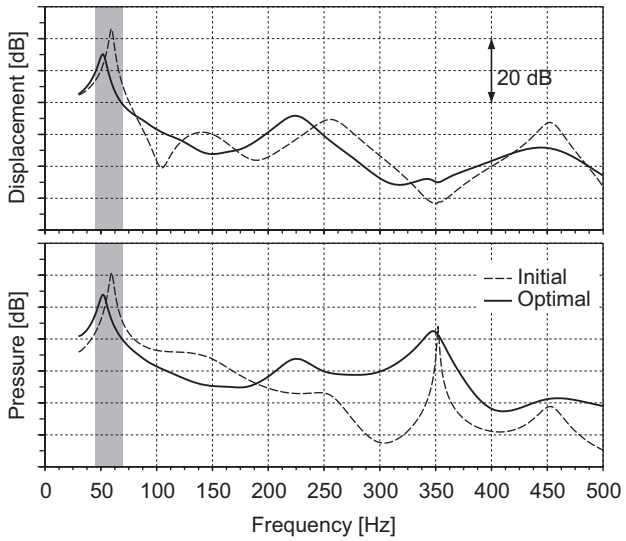

Fig. 12. Frequency response of displacement of the panel (upper) and pressure in the cavity (lower) obtained by finite element solution. Dashed line shows the initial uniform thickness and solid line shows the optimal thickness distribution for the frequency range of 45–70 Hz.

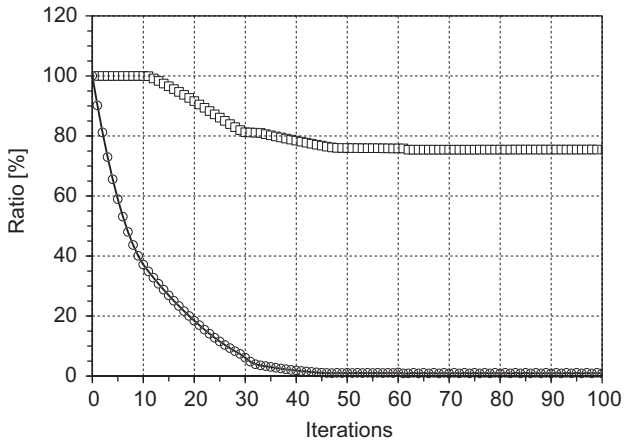

Fig. 13. Iteration histories of objective function (circle) and volume (square) for the optimization in the frequency range from 340–365 Hz.

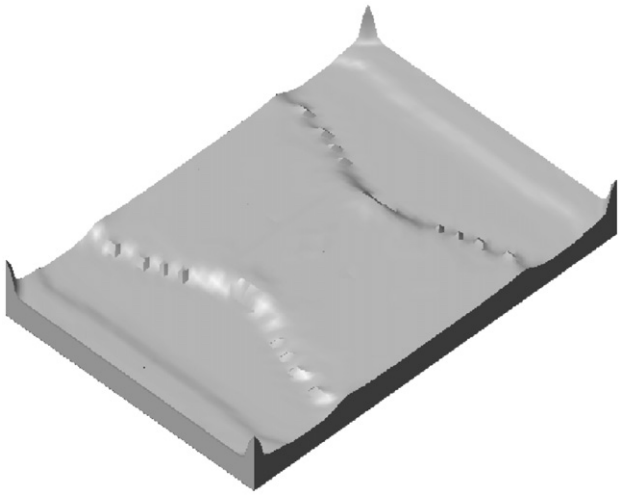

Fig. 14. Optimal thickness distribution for the optimization in the frequency range from 340–365 Hz.

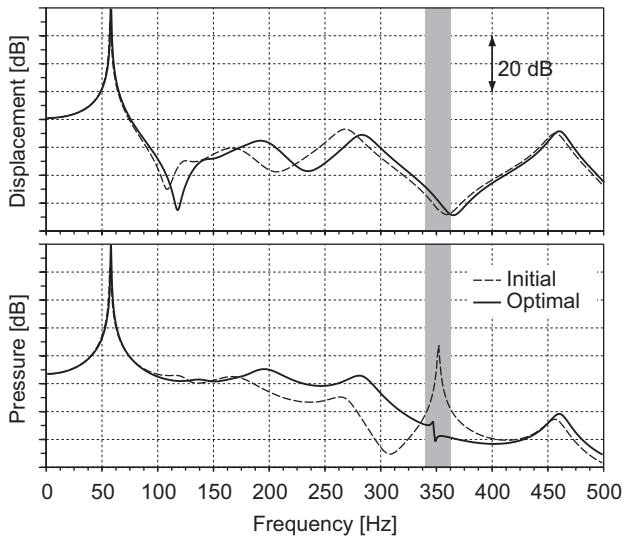

Fig. 15. Frequency response of displacement of the panel (upper) and pressure in the cavity (lower). Dashed line shows the initial uniform thickness and solid line shows the optimal thickness distribution for the frequency range of 340–365 Hz.

sound pressure response from 340 to 365 Hz in the case of the optimal thickness is less remarkable, though the response in the other frequency range is similar to the response shown in Fig. 15.

In Fig. 17, the deflection shapes of the elastic layer by transfer matrix representation are presented: (a) corresponds to the initial uniform thickness distribution and (b) to the optimal thickness distribution. Note that the area shown with a darker color has larger amplitudes of vibration. Frequencies are chosen such that the sound pressure responses in the cavity reach the maximum level within the target frequency range. Comparing Figs. 17(a) and (b), we can see that the reduction of the net sum of the volume displacement over the surface of the elastic layer leads to the minimization of sound pressure responses.

Fig. 18 displays the deflection shapes of the elastic layer when the multilayered structure is modeled using finite elements. We see that the shapes depicting longer wavelengths, which is affected by the vibration of the panel, are mostly similar to the shapes in Fig. 17, although the deflection modes of shorter wavelengths are superposed. Volume displacement induced by the short wavelength deflection modes are not dominant in terms of generated sound pressure, due to the acoustic cancellation over the surface. When complete acoustic

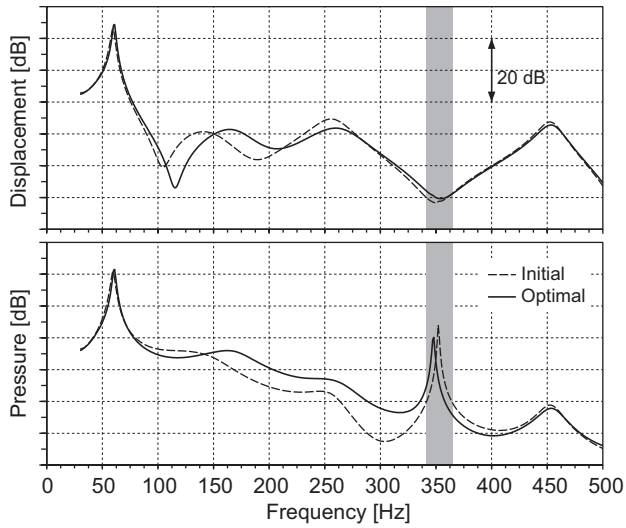

Fig. 16. Frequency response of displacement of the panel (upper) and pressure in the cavity (lower) obtained by finite element solution. Dashed line shows the initial uniform thickness and solid line shows the optimal thickness distribution for the frequency range of 340–365 Hz.

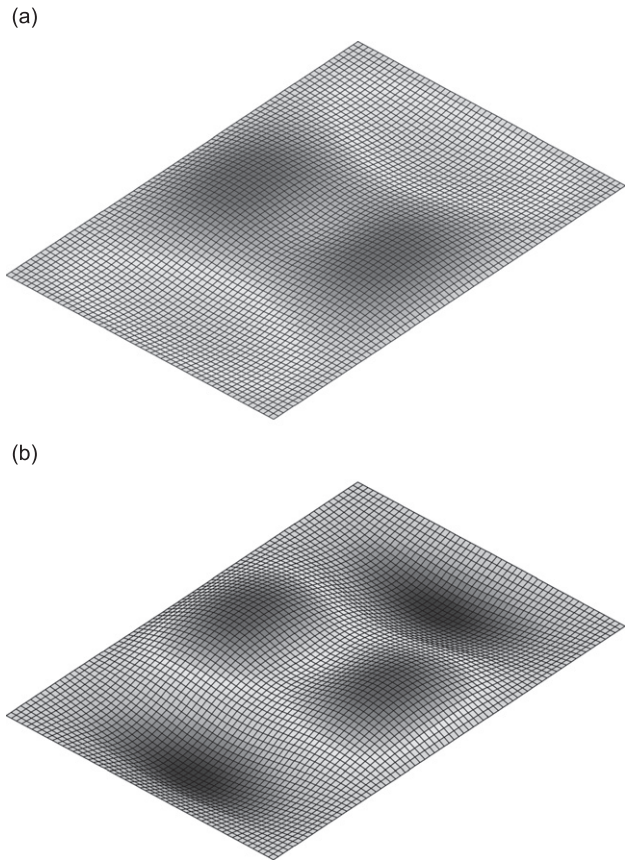

Fig. 17. Deflection shapes of elastic layer using transfer matrix representation: (a) corresponds to the initial uniform thickness at 352 Hz and (b) to the optimal thickness distribution at 346 Hz.

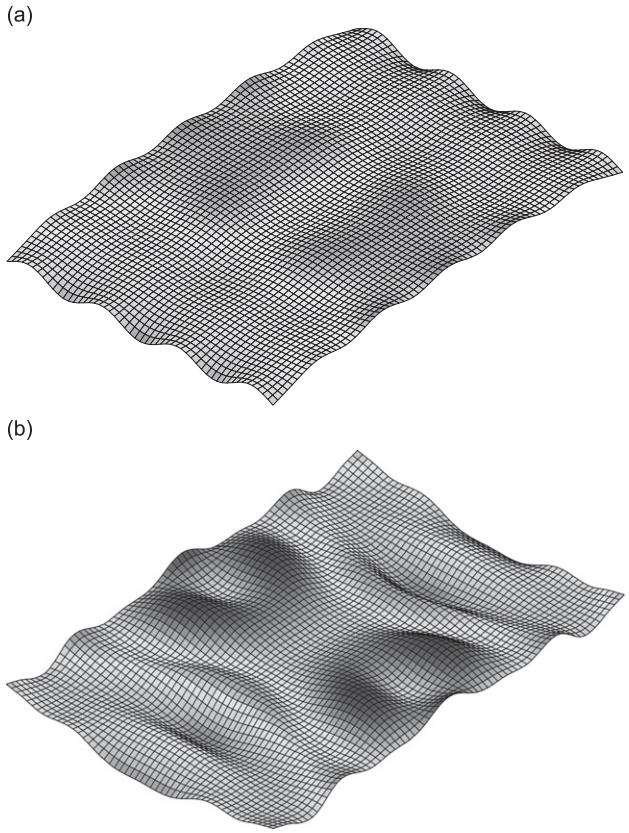

Fig. 18. Deflection shapes of elastic layer using finite element representation: (a) corresponds to the initial uniform thickness at 352 Hz and (b) to the optimal thickness distribution at 348 Hz.

cancellation is expected, as in the case shown in Fig. 17(b), detailed representations using finite elements rather than a transfer matrix is required. However, as one can see by comparing Figs. 15 and 16, the transfer matrix approach gives a good estimation of the performance across most frequency ranges.

5. Conclusions

In this paper, we developed a new design method to optimize the thickness distribution of a multilayered structure located on the coupling surface between a structure and an acoustic cavity. We conclude the following:

(1) The one-dimensional transfer matrix representation for a multilayered structure located between a structure and an acoustic cavity was incorporated into a structural–acoustic coupled problem. The approximated solution reduced computational costs significantly compared to the solution by the finite element representation, while preserving practical accuracy.
(2) A new design method to optimize thickness distribution was proposed by utilizing the concept of the density approach in topology optimization and the transfer matrix representation for a multilayered structure. The problem to minimize sound pressure levels in prescribed frequency ranges was formulated to optimize the thickness distribution of a poroelastic layer in a multilayered structure.
(3) The optimal thickness distributions in the example configurations computed by the proposed method could reduce sound pressure levels, while the volume of the multilayered structure did not increase. This confirmed that the proposed optimization method is an effective and a practical method that can be used to design multilayered structures incorporating desired performance attributes.

References

[1] K.T. Cheng, N. Olhoff, An investigation concerning optimal design of solid elastic plates, *International Journal of Solids and Structures* 17 (1981) 305–323.

[2] H.A. Eschenauer, N. Olhoff, Topology optimization of continuum structures: a review, *Applied Mechanics Reviews* 54 (2001) 331–390.

[3] C.A. Soto, A.R. Díaz, On the modelling of ribbed plates for shape optimization, *Structural Optimization* 6 (1993) 175–188.

[4] A.R. Díaz, R. Lipton, C.A. Soto, A new formulation of the problem of optimum reinforcement of Reissner–Mindlin plates, *Computer Methods in Applied Mechanics and Engineering* 123 (1995) 121–139.

[5] L.A. Krog, N. Olhoff, Optimum topology and reinforcement design of disk and plate structures with multiple stiffness and eigenfrequency, *Computers and Structures* 72 (1999) 535–563.

[6] F. Belblidia, J.E.B. Lee, S. Rechak, E. Hinton, Topology optimization of plate structures using a single- or three-layered artificial material model, *Advances in Engineering Software* 32 (2001) 159–168.

[7] L. Tenek, I. Hagiwara, Optimal rectangular plate and shallow shell topology using thickness distribution or homogenization, *Computer Methods in Applied Mechanics and Engineering* 115 (1994) 111–124.

[8] S.J. Lee, J.E. Bae, E. Hinton, Shell topology optimization using the layered artificial material model, *International Journal for Numerical Methods in Engineering* 47 (2000) 843–867.

[9] N.L. Pedersen, On topology optimization of plates with prestress, *International Journal for Numerical Methods in Engineering* 51 (2001) 225–239.

[10] O. Sigmund, J. Petersson, Numerical instabilities in topology optimization: a survey in procedures dealing with checkerboards, mesh-dependencies and local minima, *Structural Optimization* 16 (1998) 68–75.

[11] M.P. Bendsøe, O. Sigmund, *Topology Optimization—Theory, Methods and Applications*, Springer, Berlin, 2003.

[12] R.B. Haber, C.S. Jog, M.P. Bendsøe, A new approach to variable-topology shape design using a constraint on perimeter, *Structural Optimization* 11 (1996) 1–12.

[13] F. Niordson, Optimal design of elastic plates with a constraint on the slope of the thickness function, *International Journal of Solids and Structures* 19 (1983) 141–151.

[14] K. Matsui, K. Terada, Continuous approximation of material distribution for topology optimization, *International Journal for Numerical Methods in Engineering* 59 (2004) 1925–1944.

[15] S.F. Rahmatalla, C.C. Swan, A Q4/Q4 continuum structural topology optimization implementation, *Structural and Multidisciplinary Optimization* 27 (2004) 130–135.

[16] J.S. Lamancusa, Numerical optimization techniques for structural–acoustic design of rectangular panels, *Computers and Structures* 48 (4) (1993) 661–675.

[17] H.-W. Wodtke, J.S. Lamancusa, Sound power minimization of circular plates through damping layer placement, *Journal of Sound and Vibration* 215 (5) (1998) 1145–1163.

[18] J. Du, N. Olhoff, Minimization of sound radiation from vibrating bi-material structures using topology optimization, *Structural and Multidisciplinary Optimization* 33 (2007) 305–321.

[19] G.H. Yoon, J.S. Jensen, O. Sigmund, Topology optimization of acoustic–structure interaction problems using a mixed finite element formulation, *International Journal for Numerical Methods in Engineering* 60 (2006) 1049–1075.

[20] J.S. Lee, E.I. Kim, Y.Y. Kim, J.S. Kim, Y.J. Kang, Optimal poroelastic layer sequencing for sound transmission loss maximization by topology optimization method, *Journal of Acoustical Society of America* 122 (4) (2007) 2097–2106.

[21] M.A. Biot, Theory of propagation of elastic waves in a fluid-saturated porous solid. I. Low-frequency range, *The Journal of Acoustical Society of America* 28 (2) (1956) 168–178.

[22] D.L. Johnson, J. Koplik, R. Dashen, Theory of dynamic permeability and tortuosity in fluid-saturated porous media, *Journal of Fluid Mechanics* 176 (1987) 379–402.

[23] Y. Champoux, J.F. Allard, Dynamic tortuosity and bulk modulus in air-saturated porous media, *Journal of Applied Physics* 70 (4) (1991) 1975–1979.

[24] J.F. Allard, *Propagation of Sound in Porous Media*, Elsevier Applied Science, 1993.

[25] Y.J. Kang, J.S. Bolton, Finite element modeling of isotropic elastic porous materials coupled with acoustical finite elements, *Journal of Acoustical Society of America* 98 (1) (1995) 635–643.

[26] V. Easwaran, W. Lauriks, J.P. Coyette, Displacement-based finite element method for guided wave propagation problems: application to poroelastic media, *Journal of Acoustical Society of America* 100 (5) (1996) 2989–3002.

[27] N. Atalla, R. Panneton, P. Debergue, A mixed displacement–pressure formulation for poroelastic materials, *Journal of Acoustic Society of America* 104 (3) (1998) 1444–1452.

[28] J.D. Achenbach, *Wave Propagation in Elastic Solid*, North-Holland, Amsterdam, 1973.

[29] J.F. Allard, Y. Champoux, C. Depollier, Modelization of layered sound absorbing materials with transfer matrices, *Journal of Acoustical Society of America* 82 (5) (1987) 1792–1796.

[30] W. Lauriks, P. Mees, J.F. Allard, The acoustic transmission through layered systems, *Journal of Sound and Vibration* 155 (1) (1992) 125–132.

[31] M.P. Bendsøe, Optimal shape design as a material distribution problem, *Structural Optimization* 1 (1989) 193–202.